Composites Part B 138 (2018) 256–264

Contents lists available at ScienceDirect

Composites Part B

journal homepage: www.elsevier.com/locate/compositesb

Effects of polyvinyl alcohol nanofiber mats on the adhesion strength and fracture toughness of epoxy adhesive joints

Mürsel Ekrem[a,*], Ahmet Avcı[b]

[a] Mechanical Engineering Department, Necmettin Erbakan University, Konya, 42140, Turkey
[b] Mechanical Engineering Department, Selcuk University, Konya, 42075, Turkey

ARTICLE INFO

Keywords:
Polymer-matrix composites (PMCs)
Fracture toughness
Fibre/matrix bond
Wettability
Mechanical testing

ABSTRACT

The brittle nature of the polymer based adhesive joints is the major drawback limiting the service life. In this study, electrospun polyvinyl alcohol (PVA) nanofiber mat were introduced within the epoxy adhesive joint region to improve mechanical performance of the joints. The epoxy resin wetted electrospun PVA nanofiber mat were placed in between aluminum adherends and cured uncer vacuum conditions to remove air bubbles and volatiles. The mechanical performance of the reinforced aluminum joints was investigated by utilizing single lap joint (SLJ) and double cantilever beam (DCB). To reveal nano- and micro-scale toughening mechanics of the nanofiber reinforcements, the fracture surfaces were analysed using scanning electronmicroscope (SEM). Mod I fracture toughness and lap shear strength of the adhesively bonded joints were found to increase with addition of PVA nanofiber mats into epoxy adhesive.

1. Introduction

Adhesive bonding is considered as one of the most important class of joining which can be implemented diverse of laminar substrates such as metallic to metallic, metallic to composites and composites to composites [1]. Hence, adhesively bonded joints are particularly prefered in the aerospace, automative and construction industries [2–6]. Over the past decade, epoxy based adhesives getting attention of researchers due to their low shrinkage upon high dimensional stability for high performance adhesives and play a crucial role in several engineering fields [7]. Besides the advantages of adhesion technology, the epoxy based adhesive joints are often limited with having brittle nature towards crack propagation [8]. Thus, failure behavior of the adhesive bonding under static and dynamic loading conditions can also play a tremendous role in critical load bearing structures. In addition, it is very difficult to investigate the crack propagation of the joint damage with destructive test methods [9].

Various strategies have been reported in literature to enhance the mechanical performance of the epoxy adhesives [10–12]. Among these studies, the modifiying with rubber particles is an effective approach to improve energy absorbance capacity the epoxy adhesives. Recently, mechanical performance of the epoxy adhesives is increased by reinforcing nanoparticles such as carbon nanotubes (CNTs), alumina, TiO_2 nano particles [13–15]. In the case of nanoparticle reinforcement of epoxy adhesives, the mechanical performance is greatly governed by the chemical interaction between the epoxy groups and active surface groups of the functionalized nanoparticles [16–18].

As an alternative, the introduction of tough nanofibrous reinforcements between adherent laminates can be a practical way to improve the load absorbtion capacityby toughening the matrix-rich region. The nanofibrous reinforcements offer a large surface area to volume ratio, flexibility, and better mechanical performance compared to bulk polymer. Electrospinning technique affords fabrication of different kinds of polymer nanofibers with an individual fiber diameter ranging from nanometer to micrometer [19–23]. Various types of polymers have been adopted to prepare nanofibers such as polyvinyl alcohol (PVA), polyvinylpyrolidone (PVP), polyacrolanitryl (PAN), polyurethane (PU) etc [24–29]. Electrospun nanofiber mat have been recently utilized to reinforce matrix rich regions of fiber reinforced laminated composites [30–34]. Specifically, the introduction of polymer based nanofiber mat mainly contributed on fracture toughness due to existance of additional micro-mechanic toughening mechanisms depending on the nanofiber orientation.

In recent years fracture mechanics has been successfully implemented to many engineering problems. The damage tolerance design concept, essentially adopted in the aviation and space industry, was based mainly on the well-established concept of linear elastic fracture mechanics, and it has gradually gained ground in other engineering fields. The most widely used adhesively bonded joint configuration to test the resistance to Mode I cracking is the double cantilever beam

* Corresponding author. Tel.: +90 555 484 5443.
E-mail addresses: mekrem@konya.edu.tr, mekrem25@hotmail.com (M. Ekrem).

https://doi.org/10.1016/j.compositesb.2017.11.049
Received 24 January 2017; Received in revised form 7 November 2017; Accepted 29 November 2017
Available online 01 December 2017

(DCB) specimen. Many studies dealing with adhesively bonded joints use the strain energy release rate (G), and critical values for the Mode I fracture energy (G_{IC}) [35,36]. From this test, both the resistance to crack initiation and propagation can be determined and the resistance curve (plot of G_{IC} vs. crack length) can be produced. The specimen is very simple, inexpensive to fabricate and is excellent for screening adherend surface quality. In this test the substrates, usually made from metal, are bonded together with the adhesive and the crack is propagated along the adhesive layer in opening mode by pin loading at the beam-ends.

To the best of our knowledge, utilization of electrospun nanofiber mat within polymer adhesive joints has not been reported before. PVA electrospun nanofiber mat were employed to reinforce polymer resin between two adherends. Here in, the PVA nanofiber mat were fabricated via electrospin technique and following wetted with epoxy resin to use as adhesive. The chemical characteristics of the electrospun nanofiber reinforced epoxy adhesives were examined by Fourier transform infrared spectroscopy (FTIR). Furthermore, the adhesive strength and toughness were examined by single lap joint (SLJ) configurations for use with aluminum alloy 2024-T3 adherends. The effect of PVA nanofiber mat reinforcement on the interlaminar fracture toughness of the adhesively bonded joints was determined by double cantilaver beam (DCB) tests. The failure mechanisms and the damage growth were evaluated under static loading test conditions and supported with SEM analysis.

2. Theory

2.1. Simple linear elastic analysis in single lap joint

One of the most common adhesively bonded joints in practice is single lap joints, which are used in many applications as the simplest and most effective analysis. In this analysis, the adhesive only undergoes deformation in the direction of shear and the bonded materials are regarded as rigid. Peel stresses in eccentric loads are neglected. Stress analysis of single lap joints has been investigated by many researchers for a long time [37–40]. As shown in Fig. 1, the shear stress (τ) of the adhesive is constant over the overlapping length (ℓ) and is calculated by the following formula.

$$\tau = \frac{P}{b_a \ell} \tag{1}$$

where P is the applied force, b is the width of the joint.

The displacement of the adhesive from the tensile tests (with the help of dynamic extensometer, Fig. 4b) under static loading can be obtained as δ_a. Here, the shear strain (γ),

$$\gamma = \frac{\delta_a}{t_a} \tag{2}$$

where δ_a is the axial displacement of the adhesive with respect to the shear plane and t_a is the thickness of the adhesive. For shear stress (τ) and shear modulus (G),

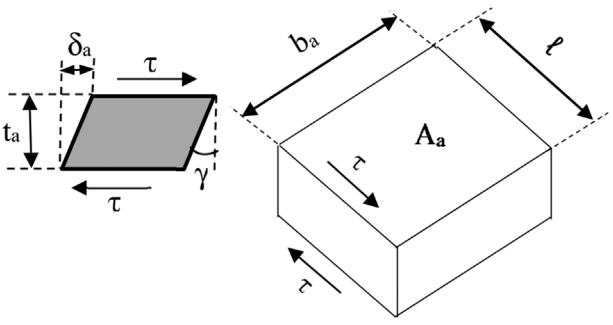

Fig. 1. Deflection of shear element.

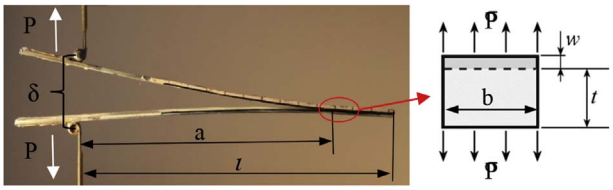

Fig. 2. Schematic representation of the DCB specimen.

$$\gamma = \frac{\tau}{G} \tag{3}$$

$$\tau = \frac{P}{A_a} \tag{4}$$

where A_a is the shear area of the adhesive ($\ell x b_a$) and P is the tensile load applied to the bonded material.

2.2. Mode-I fracture toughness

Structural modeling is the use of an alternative fracture mechanics. The success of this method is critically dependent on the actual fracture processes occurring in the adhesive. Mode I, Mode II, and mixed mode studies have been reviewed by many authors to characterize fracture durability under adhesive loading conditions with adhesive [36,41]. Double Cantilever Beam tests (DCB/Mode I) is the most commonly used method to measure the fracture toughness.

An initial region without adhesive is considered to be the pre-crack, a, and h is the adherends thickness and t is the adhesive thickness (Fig. 2.). During the test, the load P and displacements δ are registered for each crack length.

The fracture toughness values are obtained at maximum loads, before sudden crack propagation occurs and load reduction happens. If the fracture toughness values are not obtained at crack initiation positions and other non-critical positions (arrest load positions) are also included, fracture toughness can be underestimated [42]. As the aluminum adherends materials show unstable crack propagation, an incremental test method for mode I fracture testing (crack initiation - unstable crack propagation-arrest load-stable crack propagation) was also used in aluminum materials having four different situations. Crack initiation where the sudden crack growth starts, crack arrest where the crack propagation is stopped after load reduction and stable crack where a stable crack growth is observed. The fracture toughness values are obtained at crack initiation and crack arrest positions. From obtained data the Mode I interlaminar fracture toughness G_{iC} (from load to start crack) was calculated using the following equation.

$$G_{iC} = \frac{4P_{max}^2(3a^2 + h^2)}{Eb^2h^3} \tag{5}$$

and G_{aC} (from arrest load) as follows,

$$G_{aC} = \frac{4P_{min}^2(3a^2 + h^2)}{Eb^2h^3} \tag{6}$$

where P_{max} and P_{min} is the load which initiates and arrests the crack (N), E is tensile modulus of the adherend (MPa), b is the specimen width (mm), a is the crack length which measures from crack tip to pin hole centers (mm) and h is the thickness of adherend (mm).

3. Experimental

3.1. Materials

PVA (molecular weight 124 000 g/mol) was purchased from Sigma Aldrich. Sodium dodecyl sulfate (SDS) was bought from Merck. Diglycidylether of bisphenol-A (DGEBA) based epoxy resin (EPIKOTE Resin MGS RIMR 235), and curing agent (EPIKURE Curing Agent RIMH 235) were supplied by Momentive (USA) as adhesive material. Al 2024-

T3 sheets supplied by Turkish Aircraft Industry (TAI) and used as adherends. The mechanical properties of the Al-alloy are given as; Young Modulus, E = 73.1 GPa, yield strength, σ_y = 348 MPa, Ultimate Strength,σ_u = 450 MPa and Poisson's Ratio,ν = 0.33.

3.2. Preparation of the electrospun PVA nanofiber mat

The electrospun nanofiber mat were spinned from SDS added PVA/water solutions. Briefly, 10 g of PVA powder (10 w/w %) was added slowly into de-ionized water and the mixture was heated up to 70 °C. After stirring for 3 h, 100 mL SDS/water solution (1 w/w %) by was added to the PVA solution to reduce the surface tension during spinning. The PVA soluation was loaded into syringe-capillary tube with an orifis diameter 0.8 mm. The electrospinning process was utilized by applying 25 kV electrical potential between the spinneret and a collector under room temperature conditions. The gap between the spinneret and collector was fixed as 12 cm during the whole process with a fixed feed rate of 1.2 mL/h at room temperature (Univertor 801 Syringe Pump) while the collector was rotated with a speed of 10 m/s to prepare nanofiber mat. Following, the PVA nanofiber mat were removed from the drum and dried at 60 °C under vacuum for 1 h.

3.3. Preparation of aluminum adhesive joints

Surface treatment was applied to remove surface contaminants such as oil, dirt and dust and to achieve a optimum surface roughness of adhesively joint of Al sheets as shown in Fig. 3. The First, Al sheets were cut into sizes of 101.6 × 25.4 × 2 mm according to ASTM D1002 for lap joint. The bonding surfaces of the adherends were degreased by dipping in NaOH solution for 15 min at 90 °C. Following, the prepared adherends were washed with hot deionized water (50 °C) for 10 min. After washing, the adherends were put into sulfuric acid/sodium dichromate bath at 65 °C for 12 min, in accordance with ASTM D2651-01. The adherents were finally immersed into phosphoric acid anodizing solution (PAA) at room temperature according to ASTM D3933-98. The acid treated Al sheets were washed with deionized water and dried in an oven at 80 °C for 30 min. The acid treated samples were kept in desiccators for further use.

Epoxy resin system was prepared by addition of 40 wt % of the hardener into epoxy and mixed mechanically for 10 min. The presence of air bubbles in the epoxy system reduces the mechanical properties. After mixing, the resin system was placed in vacuum at room temperature for 10 min in order to remove the air bubbles. Epoxy resin mixture was placed between two Al plates, and. the PVA nanofibre mat was laid on the surface with epoxy resin of one of the adherends, subsequently. The thickness of adhesive film between adherends was controlled by using glass balls with about 220 ± 0.15 μm diameters. The bonded joints were cured at room temperature for 24 h under a curing pressure of 0.15 MPa and post cured at 80 °C for 15 h. Control samples were prepared with the same procedure without introducing PVA nanofiber mat.

3.4. Single lap joints shear strength test

Shear tests were utilized according to ASTM D 1002 standard [43]. The overlap area was fixed as 25.4 × 15 ± 0.2 mm (Fig. 4a). All mechanical tests were performed with a Instron 8801 universal tensile testing machine at room temperature with the crosshead speed of 1 mm/min. The applied load and corresponding elongation were recorded using Instron 2630-602 dynamic extensometer up to final fracture, as shown in Fig. 4b. Five samples were tested for shear strength of adherends.

3.5. Fracture toughness tests

Mode I fracture toughness were carried out according to ASTM D 3433-99 [44]. Specimens were prepared with the dimensions of 200 × 25.4 × 2 mm and a polytetrafluoroethylene film (non-adhesive) was applied in between the laminates to form pre crack as shown in Fig. 5a. Piano hinges were adhesively-bonded and tightened with three pins onto the adherends to utilize mode I loading as represented in Fig. 5b. Specimens were loaded with a constant cross-head speed rate of 1 mm/min by means of a universal test machine (Shimadzu Model AGS-X10). All the test procedure were recorded with a camera from the initial condition to the final fracture of the specimens. The video records were transferred to the computer to measure the crack opening displacement at the load point and crack growth with delamination using a proper computer program. From obtained data the Mode I interlaminar fracture toughness initial (G_{iC}) and arrest (G_{aC}) was calculated using equations (5) and (6) respectively. Five samples were tested for each set of adherends.

3.6. Measurements and characterization

Morphology of the PVA nanofiber mat and fracture surfaces of the bonded samples after mechanical tests were visualized by a ZEISS Evo LS 10 scanning electron microscope (SEM). Infrared data were collected on a Bruker Vertex 70 Fourier transform infrared (FTIR) spectroscopy in attenuated total reflectance mode using 4 scans at 2 cm^{-1} resolution and between 500 cm^{-1} and 4000 cm^{-1}. The glass transition temperature and the specific heat capacity were measured by differential scanning calorimetry (DSC, Perkin Elmer Instruments) purged with a constant nitrogen flow rate of 20 mL/min. The temperature range was set as 25–400 °C with heating rate of 20 °C/min. The surface roughness of the fracture surfaces were measured by using Mitutoyo SJ-301 for cut off distance of 7 mm. Wettebility of the epoxy resin with PVA nanofiber mat was analysed with KRUSS Easy Drop type contact angle analyzer while measuring of contact angle between PVA nanofiber mat and epoxy on the surface of Al plate.

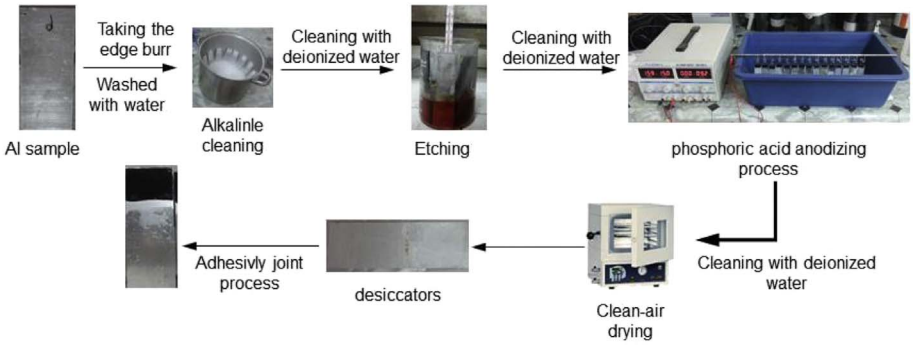

Fig. 3. Surface treatment of the aluminum adherend samples.

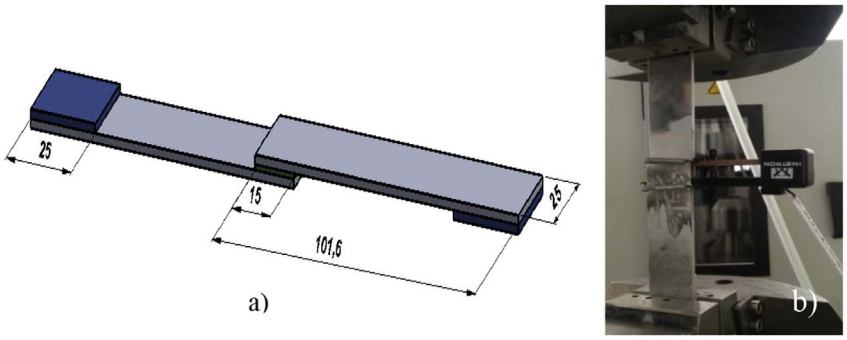

Fig. 4. Single lap joint tests a) schematic view (dimensions in mm) and b) dynamic extensometer during loading.

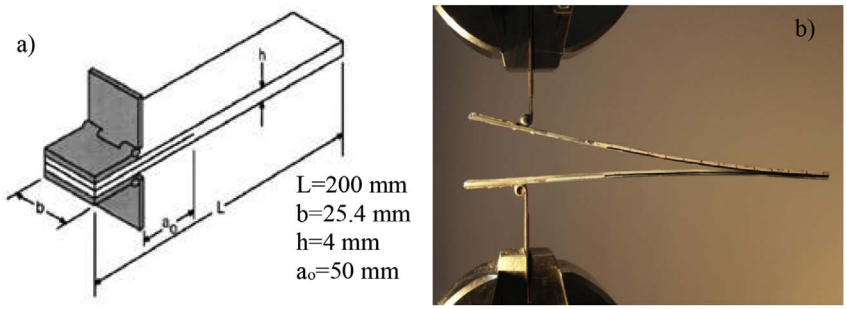

Fig. 5. Mode I loaded views of double cantilever beam test specimen a) schematic and b) crack growth during loading.

4. Results and discussion

4.1. SEM analysis of PVA nanofiber mats

Morphology of the PVA electrospun nanofiber mat strongly depends on the electrospinning parameters including applied voltage, distance between tip and collector, concentration, surface tension of PVA and feed-mass ratio. Fig. 6 a shows the SEM image of PVA electrospun nanofiber mat with several millimeters in length and about 100–200 nm in diameters. The inset represents details of the PVA nanofiber mat morphology of the as the fibers are smooth and contain a few large size of beads due to the resistance of the jetto enlarging flow [45]. Fig. 6 b shows the cross-section of PVA electrospun nanofiber mat introduced in the epoxy adhesive region. According to the SEM measurements, the thickness was measured about 120–150 μm.

4.2. FTIR of PVA nanofiber mats

The FTIR spectra of the cured neat epoxy adhesive and epoxy modified with PVA nanofiber mat adhesive are presented in Fig. 7 where transmittance (in arbitrary units) is presented as the function of wave number (cm^{-1}). The characteristic bending vibration band of the methyl groups (-CH_3) at 1384 cm^{-1} indicates of bisphenol-A and the methylene (-CH_2-) portions of epichlorohydrine appear at 1459 cm^{-1}. The epoxy has characteristic broad peak with OH group at 3000 to 3500 cm^{-1}. In addition, the epoxy exhibits three characteristic broad bands in the fingerprint region at 828, 1035 and 1250 cm^{-1}.

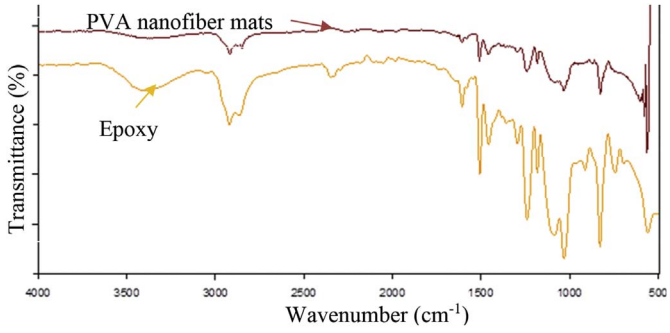

Fig. 7. FTIR spectra of the cured neat epoxy and PVA nanofiber mat modified adhesives.

PVA electrospun nanofiber mat show that the characteristic broad bands of PVA consist at 764-2850 cm^{-1} for rocking of CH, bending of CH_2, stretching of CO, bending of OH, symmetric stretching of CH_2 and asymmetric stretching of CH_2 groups [46]. The broad band of C-C stretching group of PVA at 1085 cm^{-1} adress crystallinity [47]. It is clearly seen that the band intensity in the PVA nanofiber mat at 1085 cm^{-1} comparing with neat epoxy reduces significantly in the form of a shoulder. So, we concluded from FTIR study that there was interaction occurs between neat epoxy with PVA nanofiber mat after

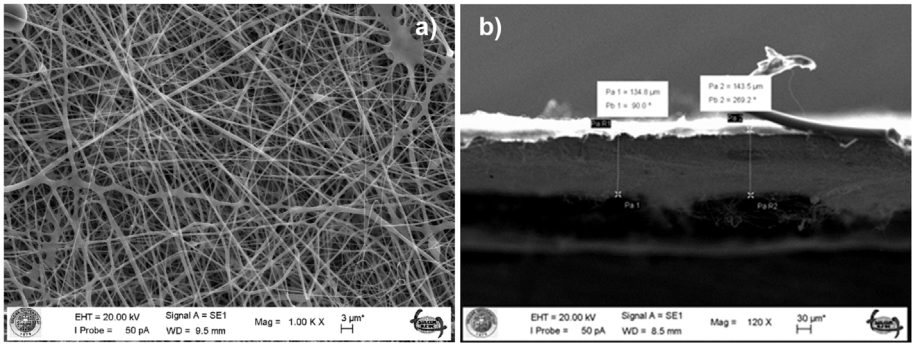

Fig. 6. a) SEM image of PVA nanofiber mat and b) thickness of PVA nanofiber mat act as nano adhesive.

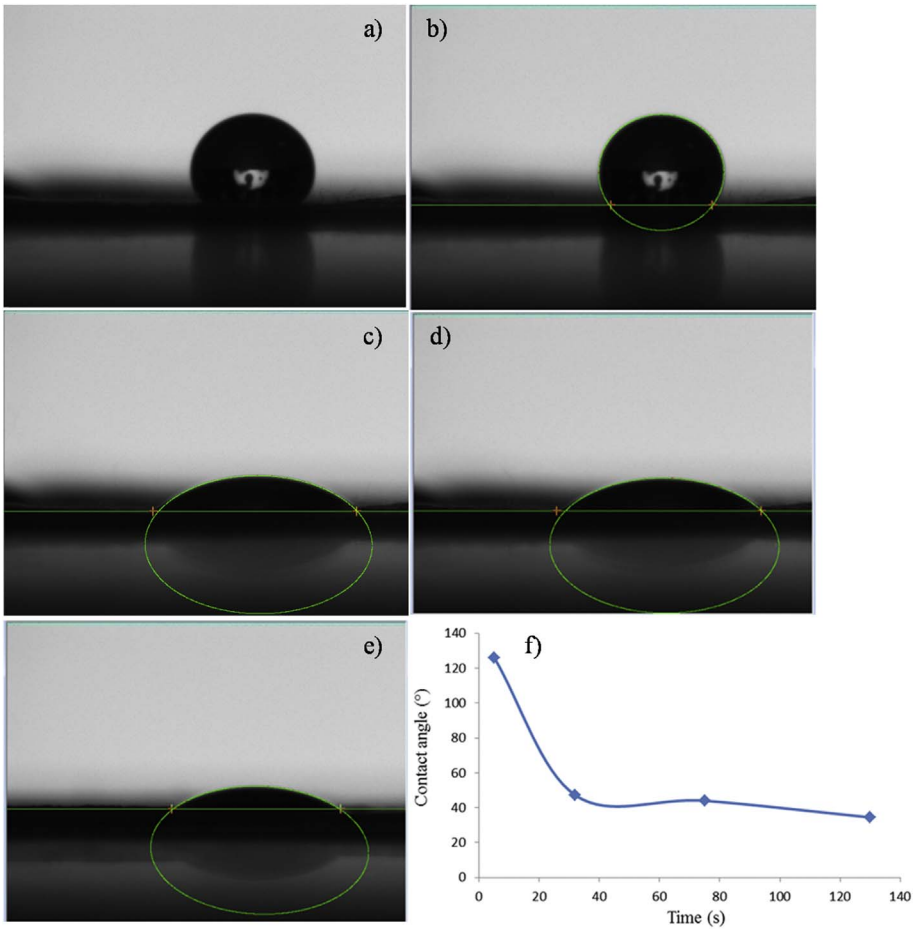

Fig. 8. (a,b,c,d,e) Wettability shapes of an epoxy droplet on the surface of the PVA nanofiber mat on aluminum substrate with respect to time, and (f) Variation of the contact angle with time.

modification.

4.3. Wettability of PVA nanofiber mat

Wettability studies usually involve the measurement of contact angles as the primary data, which indicates the degree of wetting when a solid and liquid interact [48]. Narrow contact angles (< 90°) correspond to high wettability, while wide contact angles (> 90°) correspond to low wettability. Surface charge, hydrophilicity and wettability govern the performance of adhesive joints. Fig. 8 shows the contact angle between epoxy resin and PVA nanofiber mat measured by the droplet on the PVA nanofiber mat surface on the aluminum precursor.

A drop of epoxy was placed on the PVA nanofiber mat, the contact angle was measured as 126° after 5 s and the contact angle rapidly decreased to 47° within 32 s, and the slow decreasing of the contact angle was continued and finally reached to 34.5° after130 s (Fig. 8 b). The final contact angle is less than 90° which indicates the PVA nanofiber mat can be characterized as very hydrophilic and wettable by the epoxy resin. On the basis of the work of adhesion between a solid surface (PVA nanofiber mat) and liquid (Epoxy resin) can be given as [49,50].

$$W_{sl} = \Upsilon_l(1 + \cos\theta) \quad (7)$$

where Υ_1 is the surface energy of the epoxy resin which is 46.2 mJ/m^2 [50], θ is the contact angle between solid and liquid which is 34.5° for this study. According to equation (7), the work of adhesion between the PVA electrospun nanofiber mat and the epoxy resin was calculated as 84.27 mJ/m^2. On the basis of this result, we conclude that PVA nanofiber mat and the epoxy are well adheres to each other.

4.4. Adhesive strength of single lap joints

In order to evaluate the adhesive strength of the adhesively bonded 2024-T3 Al plates, two sets of adhesives were prepared and tested such as (a) neat epoxy and (b) PVA nanofiber mat reinforced epoxy. The variation of shear stress-shear strain diagram of each group of adhesive single lap joints has been shown in Fig. 9.

Both of the neat epoxy and PVA nanofiber mat reinforced epoxy samples represent a linear elastic behavior until failure. The average shear strength of neat samples is calculated to be 20.81 ± 1.00 MPa and shear strain of 11.57 ± 2.00 mm/mm, while the PVA nanofiber mat reinforced epoxy adhesive exhibits higher performance since the

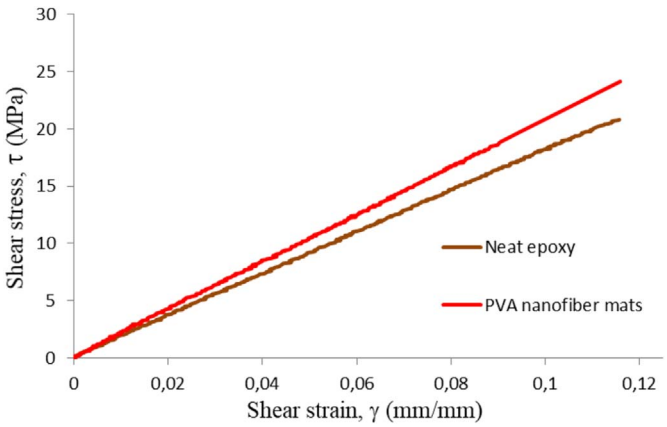

Fig. 9. Variation in shear stresses as a function of shear strains for neat epoxy adhesive and epoxy modified with PVA nanofiber mat adhesive.

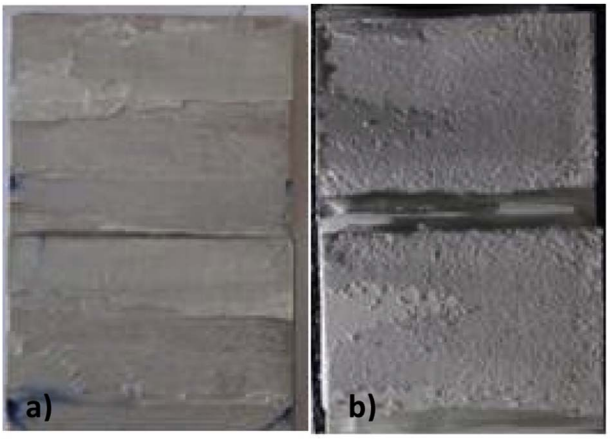

Fig. 10. Fracture surfaces of single lap joints (a) epoxy, (b) epoxy with PVA nanofiber mats.

shear strength is increased by 13.50% strength. Clearly, almost no obvious change in the shear strain values was observed with the introduction of PVA nanofiber mat. It is concluded that the epoxy resin system containing PVA mat exhibits a dramatic increase in adhesive strength of lap jointed with Al adherends.

The PVA nanofiber mat reinforced epoxy adhesives also exhibit improved shear modulus. It is calculated that the shear modulus is increased by about 29% compared to the neat epoxy adhesive. It is apparent that the resulting structure is a good candidate for decreasing the brittleness of the epoxy adhesive (Fig. 10).

Fig. 11 shows SEM images of the neat epoxy and epoxy with PVA nanofiber mats adhesives from the fractured surfaces of the single lap joint tension tests. As shown in Fig. 11 a, the neat epoxy adhesive displayed a smooth and featureless surface, typical of brittle fracture of homogenous thermoset polymers. Fig. 11 b shows the dispersion of PVA nanofiber mat in epoxy adhesive with well imregnation. Moreover, the inclined failure mode is observed with cohesive adhesive for neat epoxy adhesive in Fig. 11 a. The epoxy adhesive containing PVA electrospun nanofiber mat reveals a significant increase in strength and stiffness, due to resistance of fracture. Additionally the PVA nanofiber mat resists the formation of crack path. The epoxy adhesive modified by PVA nanfiber mat reduces the crack initiation and propagation by bridging or crack arresting. The fiber bridging shown in Fig. 11 b is in good agreement with the bridging mechanisms were prior explained for enhancing the fracture toughness in various researches [51,52] as epoxy modified with carbon nanotubes.

4.5. DCB fracture tests of adhesive systems

4.5.1. Mode I interlaminar fracture toughness investigations

Fig. 12 a shows typical mode-I load versus load point displacement curves for DCB specimens of the neat epoxy and the epoxy with PVA nanofiber mat reinforced epoxy adhesive systems. For both type of specimens the load increases until the crack initiation process is completed and then the crack starts to propagate. It is revealed that the types of crack propagations are unstable followed by stable growth with the distinct sudden dropped load versus displacement curves.

The initial responses of the neat epoxy and the epoxy with PVA fiber mat adhesive samples exhibit almost linear behavior. All samples represent stick–slip crack growth since; there exist an air gaps in the adhesive, non uniform adhesive materials along the jointed area and partly weak bonds between adhesive and adherend. The maximum peak loads of the load-load point displacement curves are related with the onset of the crack growth. The lower values of the loads represent the barrier of the unstable crack growth.

For the DCB specimens of PVA nanofiber mat reinforced epoxy adhesive system, the length of the unstable crack growth was much greater than neat epoxy adhesive since the higher pick loads for crack propagation were achieved.

As it is seen from Fig. 12 a, the load versus load point displacement curves for both of the samples show sharp and suddenly drops in loads with unstable crack growth while increasing load point displacement.

The numer of sudden drops and corresponding unstable crack growth of epoxy with PVA nanofiber mats adhesive system are greater than those of neat epoxy adhesive. This indicates that the PVA electrospun nanofiber mats improve the interface bonding of the adhesive joint of aluminum adherends. In Fig. 12 b the load is seen to decrease with rapid increasing crack length from the maximum level of the loads for both adhesive systems. But it is clear from this diagram that loads are increasing to a certain level with a slow increasing crack length during arrest phases. This step changing of the loads commonly referred to as stick-slip growth. The results show a reduction on the fracture toughness propagation value when a crack initiation - unstable crack propagation-arrest load-stable crack propagation is applied. In Fig. 12 a, when the load point displacement Pmax decreases vertically to the load Pmin, in Fig. 12 b, the crack growth in observed as the unstable crack progression hypotenuse curve with sudden energy release. Thus, the crack growth is approximately 3 times the load point displacement.

According to the curves of adhesive systems in Fig. 13 two critical strain energy release rates were calculated using equation (1). One of them is denoted with crack initiation (i.e. maximum loading level) G_{iC} and the second associated with crack arrest G_{aC}. The critical strain energy release rate results of the both adhesive systems associated with crack initiation and crack arrest are shown in Fig. 13 a and b.

The maximum mode I fracture energy, G_{iC}, of the neat epoxy adhesive for crack initiation case was calculated to be 396 J/m^2 at the final peak of the load, while the average fracture energy found to be 252 J/m^2 as would be expected for a linear brittle epoxy. The maximum fracture energy of the neat epoxy adhesive for crack arrest case was 203 J/m^2 (Fig. 13 b).

In epoxy with PVA nanfiber mats adhesive system, the maximum fracture energy was calculated to be 560 J/m^2 for crack initiation case at the third peak of the load. The average mode I fracture energy for the

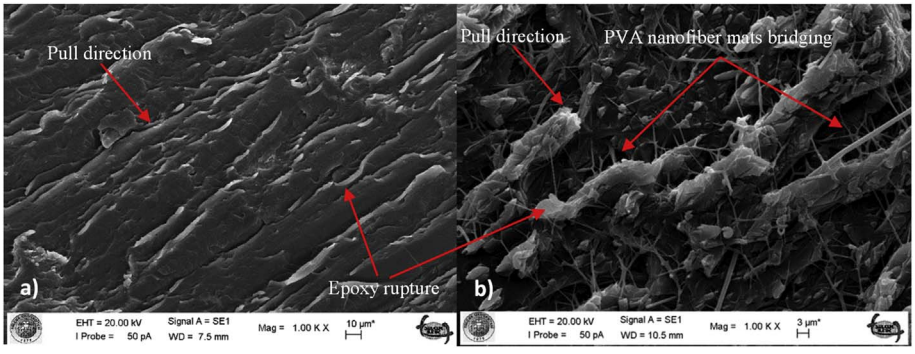

Fig. 11. SEM images of adhesives: (a) neat epoxy and (b) epoxy with PVA nanofiber mats.

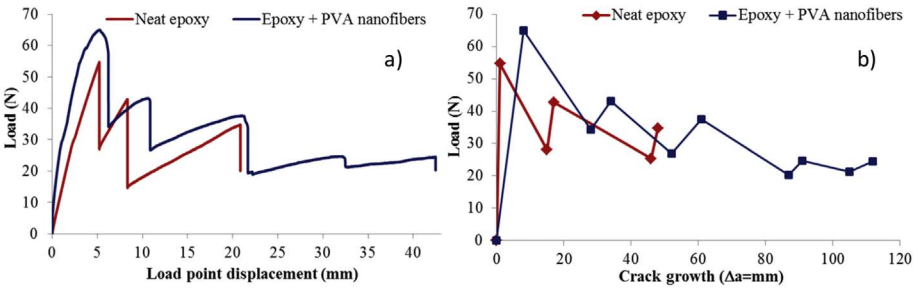

Fig. 12. (a)Typical load versus load point displacement curves and (b) The load-crack length plot for neat epoxy adhesive and epoxy with PVA nanofiber mats adhesive systems for DCB fracture tests.

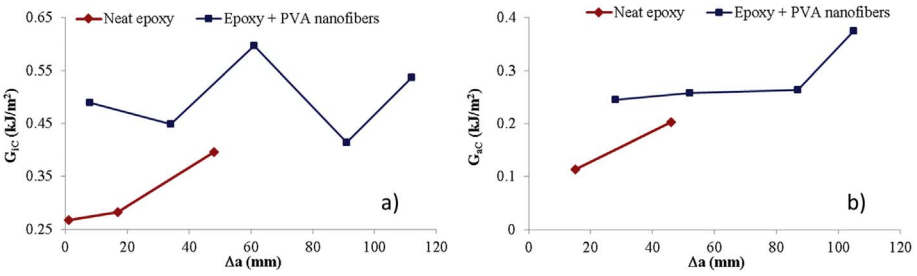

Fig. 13. The comparison of critical strain energy release rates for (a) crack initiation and (b) crack arrest for neat epoxy and epoxy with PVA nanofiber mats systems.

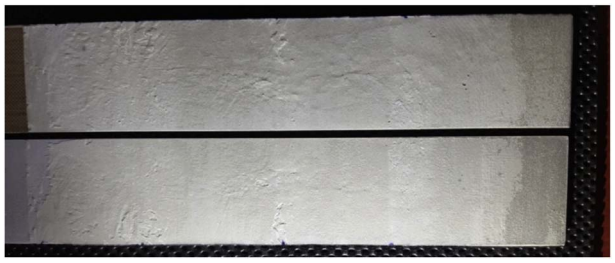

Fig. 14. Fracture surface of a DCB test specimen for epoxy with PVA nanofiber mats adhesive system.

same adhesive system was obtained to be 497 J/m^2. For the crack arrest case the maximum fracture energy was found to be 380 J/m^2 at the final stage of the crack arrest. One can observed from Fig. 13 a that the average critical strain energy of the epoxy with PVA nanofiber mats adhesive system is 97% higher than that of the critical strain energy of neat epoxy adhesive. Addition of PVA nanofiber mats in the epoxy improves the fracture toughness of the epoxy adhesive The similar improvements have been reported for CNT/epoxy nano adhesives and were suggested to be due to lack of free space available for distribution of the CNTs in the epoxy [53–55].

A typical fracture surface for the sample of the epoxy with PVA nanofiber mats adhesive system has been shown in Fig. 14. The ragions of crack initiation (stable crack extensions) and crack arrest (unstable fractures) can be seen as obvious stick-slip lines on the fracture surface of the specimen. The unstable crack extension regions are visible as darker areas than stable crack propagated ragions and show a very brittle fracture mechanism occurred.

When the applied load growing up to 65.04 kN the first stable crack extension occurres around 8 mm. Then after the first unstable crack extension happens about 20 mm with sudden dropping the applied load to the 34.22 kN. Three more similar crack extensions repeated with different amount of propagations up to joint broken with final fast fracture.

During stable and unstable crack extension the crack propagates through adhesive, unlike among the surface of the aluminum adherend and epoxy with PVA nanofiber mats adhesives.

4.5.2. SEM anaylsis of DCB tests

Figs. 15 and 16 show the SEM images of the fracture surface of the neat epoxy adhesive and epoxy with the PVA nanofiber mats adhesive system from a constant displacement rate of DCB tests at room temperature. SEM micrographs of the fracture surfaces of the adhesively joint with neat epoxy shown in Fig. 15 depict smooth fracture surfaces in different planes. This is an obvious brittle fracture for neat epoxy adhesives and it requires relatively small amount of energy for crack propagation.

A SEM image of one such local spot is shown in Fig. 16 a for the fracture surface of the epoxy with PVA nanofiber mats adhesive sample. The crack propagation path seems to either go through inside the PVA nanofiber mats or between the adhesive and Al adherend. Besidesan obvious nanofiber matrix debonding is seen on the fracture surface of the nano adhesive samples (Fig. 16 b). These tendencies are qualitatively indicative of the nanofiber mats forming some sort of an arrest to

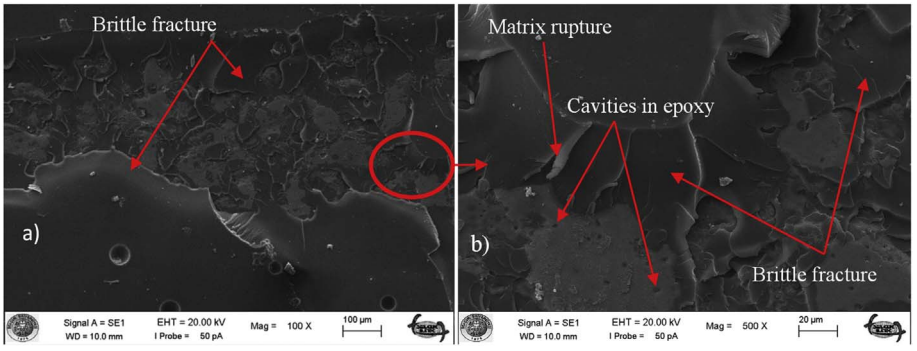

Fig. 15. SEM images of the crack initiation region of the fracture surfaces for the neat epoxy adhesive from DCB test a) 100× and b) 500×.

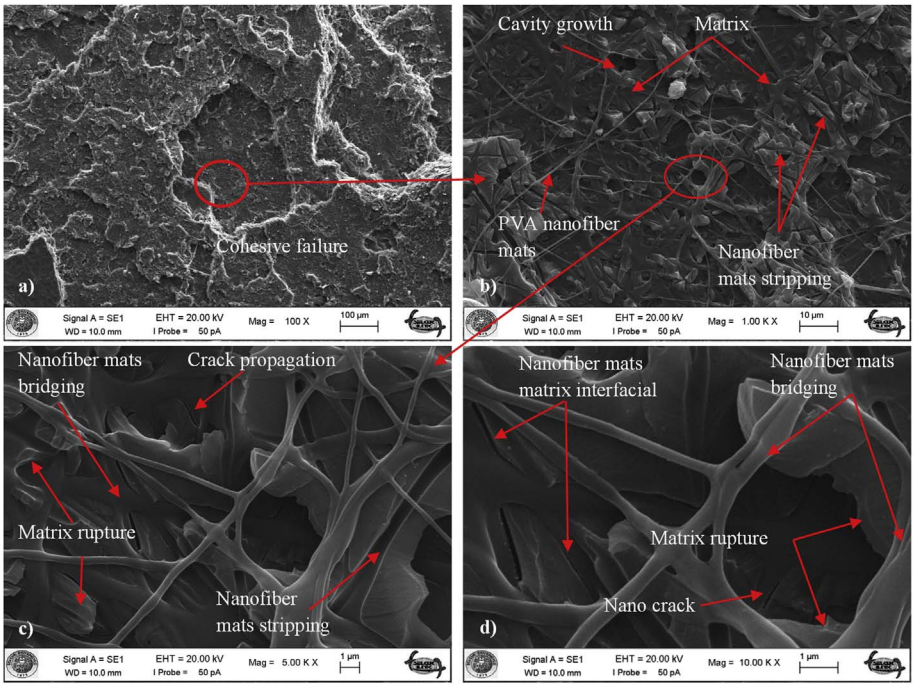

Fig. 16. SEM images of the crack initiation region of the fracture surfaces for the epoxy with PVA nanofiber mats adhesive from DCB test, a) 100 ×, b) 1000 × and c) 5000 × and d) 10 000 ×.

the propagation of the crack. A significant number of debonding grooves are seen in Fig. 15 b and are indicative of resisting to crack growth of the epoxy with PVA nanofiber mats adhesive in the process zone, which leads to increase in the fracture energy, compared to the neat epoxy adhesive. A triaxial strees field consist in the ahead of the crack tip (Fig. 16 a), therefore the PVA nanofiber mats debond from the epoxy as the local stresses rise at the crack tip. The debonding of PVA nanofiber mats, the formation of cavitie sand crack branching in the epoxy cause the polymer to deform plastically. For the epoxies toughened with rubber, nanosilica and carbon nanofibers, the plastic void formation mechanism was shown to highly increase the fracture toughness of the epoxy [56,57]. Therefore the addition of PVA nanofiber mats in the epoxy increases in the fracture energy of the epoxy adhesive system and participates the toughening mechanisms. The fracture energy dissipation can be considered with the combination of interfacial de bonding of the PVA nanofiber mats, cavity formation in the epoxy and the triaxial stress region behind the crack tip and crack branching in the epoxy.

A cohesive failure of the epoxy with PVA nanofiber mats adhesive can be seen in the SEM image in Fig. 16 c, complete with evidence of the PVA nanofiber mats in the cavities formation. On the other hand some voids are seen in the SEM images due to insufficient wetting of the PVA nanofiber mats with epoxy during bonding. The SEM observations propose a need to control the bonding process by means of a quantitative understanding of the PVA nanofiber mats dispersion in epoxy.

Therefore the addition of PVA nanofiber mats in the epoxy increases in the fracture energy of the epoxy adhesive system and participates the toughening mechanisms. The fracture energy dissipation can be considered with the combination of interfacial debonding of the PVA nanofiber mats, cavity formation in the epoxy and the triaxial stress region behind the crack tip and crack branching in the epoxy. The toughening mechanisms of the modified epoxy adhesive system with PVA nanofiber mats can be stated as the interfacial debonding of the PVA nanofiber mats generated from the epoxy resin, the energy required to pull-out the PVA nanofiber mats from the epoxy, cavity growth in the epoxy and rupturing of PVA nanofiber mats in the epoxy. The similar toughening mechanisms were explained in Ref. [58].

5. Conclusion

Adhesive strength and fracture toughness of the lap joint and DCB bonded with epoxy adhesive modified by the addition of PVA electrospun nanofiber mats were investigated. The PVA electrospun nanofiber mats were wetted with liquid epoxy by roll mill before applying adhesively joint. Then the electrospun nanofiber mats developed the adhesion capability and resistance to fracture of the epoxy adhesive. The addition of PVA nanofiber mats into the epoxy adhesive, the shear strength increased about 13.50% but the shear strain almost the same when compared with neat epoxy. It is concluded that the epoxy resin system containing PVA nanofiber mats exhibits a significant increase in adhesive strength of lap jointed with Al adherends.

The wettability of PVA nanofiber mats with epoxy showed very hydrophilic property that the adhesion work was 84.27 mJ/m^2 with the contact angle of 34.5°. The wetting behavior of PVA nanfiber mat with epoxy adhesive was offered as one of the key factor for the improved adhesion strength.

It was also seen that the epoxy adhesive reinforced with electrospun nanofibers decreased the speed of crack growth in the DCB joints. The fructure toughness of the DCB joint was found to very effective addition of PVA electrospun nanofiber mats in epoxy. The laying of PVA nanofiber mats in the epoxy adhesive led to increase the average fracture toughness G_{IC} from 252 J/m^2 to 497 J/m^2, compared to neat epoxy adhesive.

References

[1] Reis PNB, Ferreira JAM, Antunes F. Effect of adherend's rigidity on the shear strength of single lap adhesive joints. Int J Adhes Adhes 2011;31(4):193–201.
[2] May C. Epoxy resins: chemistry and technology. CRC press; 1987.
[3] Nistico N, Ozbolt J, Polimanti G. Modeling of reinforced concrete beams strengthened in shear with CFRP: microplane-based approach. Compos Part B Eng 2016;90:351–64.
[4] Mansourian-Tabaei M, Jafari SH, Khonakdar HA. Lap shear strength and thermal stability of diglycidyl ether of bisphenol a/epoxy novolac adhesives with nanoreinforcing fillers. J Appl Polym Sci 2014;131(6).
[5] Ma HL, Jia ZM, Lau KT, Li XF, Hui D, Shi SQ. Enhancement on mechanical strength of adhesively-bonded composite lap joints at cryogenic environment using coiled carbon nanotubes. Compos Part B Eng 2017;110:396–401.
[6] Orefice A, Mancusi G, Feo L, Fraternali F. Cohesive interface behaviour and local shear strains in axially loaded composite annular tubes. Compos Struct 2017;160:1126–35.

[7] Khoee S, Hassani N. Adhesion strength improvement of epoxy resin reinforced with nano elastomeric copolymer. Mater Sci Eng A Struct Mater Prop Microstruct Process 2010;527(24–25):6562–7.
[8] Lee H, Neville K. Handbook of epoxy resins. 1967.
[9] Titov SA, Maev RG, Bogachenkov AN. Pulse-echo NDT of adhesively bonded joints in automotive assemblies. Ultrasonics 2008;48(6–7):537–46.
[10] Bagheri R, Marouf BT, Pearson RA. Rubber-toughened epoxies: a critical review. Polym Rev 2009;49(3):201–25.
[11] Ghosh PK, Patel A, Kumar K. Adhesive joining of copper using nano-filler composite adhesive. Polymer 2016;87:159–69.
[12] Kang W-S, Rhee KY, Park S-J. Influence of surface energetics of graphene oxide on fracture toughness of epoxy nanocomposites. Compos Part B Eng 2017;114:175–83.
[13] Ghosh PK, Pathak A, Goyat MS, Halder S. Influence of nanoparticle weight fraction on morphology and thermal properties of epoxy/TiO2 nanocomposite. J Reinf Plast Comp 2012;31(17):1180–8.
[14] Ghosh PK, Kumar K, Chaudhary N. Influence of ultrasonic dual mixing on thermal and tensile properties of MWCNTs-epoxy composite. Compos Part B Eng 2015;77:139–44.
[15] Opelt CV, Becker D, Lepienski CM, Coelho LAF. Reinforcement and toughening mechanisms in polymer nanocomposites - carbon nanotubes and aluminum oxide. Compos Part B Eng 2015;75:119–26.
[16] Duzcukoglu H, Ekinci S, Sahin OS, Avci A, Ekrem M, Unaldi M. Enhancement of wear and friction characteristics of epoxy resin by multiwalled carbon nanotube and boron nitride nanoparticles. Tribol Trans 2015;58(4):635–42.
[17] Ulus H, Ustun T, Eskizeybek V, Sahin OS, Avci A, Ekrem M. Boron nitride-MWCNT/epoxy hybrid nanocomposites: preparation and mechanical properties. Appl Surf Sci 2014;318:37–42.
[18] Ekrem M, Ataberk N, Avcı A, Akdemir A. Improving electrical and mechanical properties of a conductive nano adhesive. J Adhes Sci Technol 2016:1–14.
[19] Wong SC, Baji A, Leng SW. Effect of fiber diameter on tensile properties of electrospun poly(epsilon-caprolactone). Polymer 2008;49(21):4713–22.
[20] Luo C, Stoyanov SD, Stride E, Pelan E, Edirisinghe M. Electrospinning versus fibre production methods: from specifics to technological convergence. Chem Soc Rev 2012;41(13):4708–35.
[21] Nezarati RM, Eifert MB, Cosgriff-Hernandez E. Effects of humidity and solution viscosity on electrospun fiber morphology. Tissue Eng Part C Methods 2013;19(10):810–9.
[22] Li Z, Wang C. Effects of working parameters on electrospinning. One-Dimensional Nanostructures. Springer; 2013. p. 15–28.
[23] Reneker DH, Chun I. Nanometre diameter fibres of polymer, produced by electrospinning. Nanotechnology 1996;7(3):216.
[24] Phong NT, Gabr MH, Okubo K, Chuong B, Fujii T. Improvement in the mechanical performances of carbon fiber/epoxy composite with addition of nano-(polyvinyl alcohol) fibers. Compos Struct 2013;99:380–7.
[25] Barzegar F, Bello A, Fabiane M, Khamlich S, Momodu D, Taghizadeh F, et al. Preparation and characterization of poly (vinyl alcohol)/graphene nanofibers synthesized by electrospinning. J Phys Chem Solids 2015;77:139–45.
[26] Moayeri A, Ajji A. Fabrication of polyaniline/poly (ethylene oxide)/non-covalently functionalized graphene nanofibers via electrospinning. Synth Met 2015;200:7–15.
[27] Sharma DK, Shen J, Li F. Reinforcement of Nafion into polyacrylonitrile (PAN) to fabricate them into nanofiber mats by electrospinning: characterization of enhanced mechanical and adsorption properties. Rsc Adv 2014;4(74):39110–7.
[28] Tijing LD, Park CH, Choi WL, Ruelo MTG, Amarjargal A, Pant HR, et al. Characterization and mechanical performance comparison of multiwalled carbon nanotube/polyurethane composites fabricated by electrospinning and solution casting. Compos Part B Eng 2013;44(1):613–9.
[29] Ekrem M. Mechanical properties of MWCNT reinforced polyvinyl alcohol nanofiber mats by electrospinnig method. El-Cezeri J Sci Eng 2017;4(2):190–200.
[30] Daelemans L, van der Heijden S, De Baere I, Rahier H, Van Paepegem W, De Clerck K. Using aligned nanofibres for identifying the toughening micro mechanisms in nanofibre interleaved laminates. Compos Sci Technol 2016;124:17–26.
[31] Saghafi H, Zucchelli A, Palazzetti R, Minak G. The effect of interleaved composite nanofibrous mats on delamination behavior of polymeric composite materials. Compos Struct 2014;109:41–7.
[32] Kim JW, Lee JS. Influence of interleaved films on the mechanical properties of carbon fiber fabric/polypropylene thermoplastic composites. Materials 2016;9(5).
[33] Hamer S, Leibovich H, Green A, Intrater R, Avrahami R, Zussman E, et al. Mode I interlaminar fracture toughness of nylon 66 nanofibrilmat interleaved carbon/epoxy laminates. Polym Compos 2011;32(11):1781–9.
[34] Palazzetti R, Zucchelli A, Gualandi C, Focarete ML, Donati L, Minak G, et al. Influence of electrospun Nylon 6,6 nanofibrous mats on the interlaminar properties of Gr-epoxy composite laminates. Compos Struct 2012;94(2):571–9.
[35] Blackman BRK, Kinloch AJ, Rodriguez-Sanchez FS, Teo WS. The fracture behaviour of adhesively-bonded composite joints: effects of rate of test and mode of loading. Int J Solids Struct 2012;49(13):1434–52.
[36] Katsiropoulos CV, Chamos AN, Tserpes KI, Pantelakis SG. Fracture toughness and shear behavior of composite bonded joints based on a novel aerospace adhesive. Compos Part B Eng 2012;43(2):240–8.
[37] Sayman O. Elasto-plastic stress analysis in an adhesively bonded single-lap joint. Compos Part B Eng 2012;43(2):204–9.
[38] da Silva LFM, das Neves PJC, Adams RD, Spelt JK. Analytical models of adhesively bonded joints-Part I: literature survey. Int J Adhesion Adhes 2009;29(3):319–30.
[39] Ganghoffer JF, Schultz J. An analytical model of the mechanical behaviour of elastic adhesively bonded joints. J Adhes 1996;55(3–4):285–302.
[40] Her SC. Stress analysis of adhesively-bonded lap joints. Compos Struct 1999;47(1–4):673–8.
[41] Chaves FJP, da Silva LFM, de Moura MFSF, Dillard DA, Esteves VHC. Fracture mechanics tests in adhesively bonded joints: a literature review. J Adhes 2014;90(12):955–92.
[42] Olave M, Vara I, Husabiaga H, Aretxabaleta L, Lomov SV, Vandepitte D. Nesting effect on the mode I fracture toughness of woven laminates. Compos Part A Appl S 2015;74:166–73.
[43] ASTM. D 1002–1010. Standard test method for apparent shear strength of single-lap-joint adhesively bonded metal specimens by tension loading (metal-to-metal). 2010.
[44] ASTM. D 3433–3499. Standard test method for fracture strength in cleavage of adhesives in bonded Metal joints. 2005.
[45] Huan SQ, Bai L, Cheng WL, Han GP. Manufacture of electrospun all-aqueous poly (vinyl alcohol)/cellulose nanocrystal composite nanofibrous mats with enhanced properties through controlling fibers arrangement and microstructure. Polymer 2016;92:25–35.
[46] Kim G-M, Asran AS, Michler GH, Simon P, Kim J-S. Electrospun PVA/HAp nanocomposite nanofibers: biomimetics of mineralized hard tissues at a lower level of complexity. Bioinspiration Biomimetics 2008;3(4):046003.
[47] Tadokoro H, Seki S, Nitta I. Some information on the infrared absorption spectrum of polyvinyl alcohol from deuteration and pleochroism. J Polym Sci 1956;22(102):563–6.
[48] Yuan Y, Lee TR. Contact angle and wetting properties. Surface science techniques. Springer; 2013. p. 3–34.
[49] Singh J, Whitten JE. Forces between polymer surfaces and self-assembled monolayers. J Macromol Sci A 2008;45(11):884–91.
[50] Bouali B, Ganachaud F, Chapel JP, Pichot C, Lanteri P. Acid-base approach to latex particles containing specific groups based on wettability measurements. J Colloid Interf Sci 1998;208(1):81–9.
[51] Srivastava VK. Effect of carbon nanotubes on the strength of adhesive lap joints of C/C and C/C-SiC ceramic fibre composites. Int J Adhesion Adhes 2011;31(6):486–9.
[52] De La Vegala A, Pradol LASD, Kovacs JZ, Bauhofer W, Schulte K. SWCNT as cure-induced stress sensors in epoxy nanocomposites. Nanocompos Mater 2009;151:48–53.
[53] Jakubinek MB, Ashrafi B, Zhang YF, Martinez-Rubi Y, Kingston CT, Johnston A, et al. Single-walled carbon nanotube-epoxy composites for structural and conductive aerospace adhesives. Compos Part B Eng 2015;69:87–93.
[54] Wernik JM, Meguid SA. On the mechanical characterization of carbon nanotube reinforced epoxy adhesives. Mater Des 2014;59:19–32.
[55] Jojibabu P, Jagannatham M, Haridoss P, Ram GDJ, Deshpande AP, Bakshi SR. Effect of different carbon nano-fillers on rheological properties and lap shear strength of epoxy adhesive joints. Compos Part A Appl S 2016;82:53–64.
[56] Williams JG. Particle toughening of polymers by plastic void growth. Compos Sci Technol 2010;70(6):885–91.
[57] Hsieh TH, Kinloch AJ, Masania K, Taylor AC, Sprenger S. The mechanisms and mechanics of the toughening of epoxy polymers modified with silica nanoparticles. Polymer 2010;51(26):6284–94.
[58] Ladani RB, Wu SY, Kinloch AJ, Ghorbani K, Zhang J, Mouritz AP, et al. Improving the toughness and electrical conductivity of epoxy nanocomposites by using aligned carbon nanofibres. Compos Sci Technol 2015;117:146–58.